High-performance near-field electroluminescent refrigeration device consisting of a GaAs light emitting diode and a Si photovoltaic cell

Kaifeng Chen,[1,2] Tianyao P. Xiao,[3] Parthiban Santhanam,[2] Eli Yablonovitch,[3,a)] and Shanhui Fan[2,b)]
[1]*Department of Applied Physics, Stanford University, Stanford, California 94305, USA*
[2]*Department of Electrical Engineering, Ginzton Laboratory, Stanford University, Stanford, California 94305, USA*
[3]*Department of Electrical Engineering and Computer Sciences, University of California, Berkeley, California 94720, USA*

(Received 28 May 2017; accepted 2 October 2017; published online 13 October 2017)

We consider a near-field electroluminescent refrigeration device. The device uses a GaAs light emitting diode as the cold side, and a Si photovoltaic cell as the hot side. The two sides are brought in close proximity to each other across a vacuum gap. The cooling is achieved by applying a positive bias on the GaAs light emitting diode. We show that the choice of GaAs and Si here can suppress the non-idealities for electroluminescent cooling purposes: GaAs has a wide bandgap with low Auger recombination, and Si is a non-polar semiconductor which leads to significantly reduced sub-bandgap heat transfer. We show that by using this configuration in the near-field regime, the cooling power density can reach $10^5\ \mathrm{W/m^2}$ even in the presence of realistic Auger recombination and Shockley-Read-Hall recombination. In addition, with photovoltaic power recovery from the Si cell, the efficiency of the device can be further improved. Our work points to the significant potential of combining near-field heat transfer with active semiconductor devices for the control of heat flow. *Published by AIP Publishing*. https://doi.org/10.1063/1.5007712

I. INTRODUCTION

In the near field, the radiative heat transfer between two planar bodies can be significantly enhanced beyond the far-field limit as described by Planck's law due to the presence of evanescent waves.[1–12] Such enhancement has been widely studied in many applications. For example, in thermophotovoltaics (TPV), the near-field heat transfer could significantly enhance the output power density as well as the efficiency.[13–19]

The concept of near-field electromagnetic heat transfer can also be used to enhance the operation of cooling devices based on electroluminescence. In 1957, Tauc proposed to use electroluminescence for cooling purposes.[20] He showed that in the ideal limit, a light emitting diode (LED) at forward bias can be used as a cooling device that removes the entropy from its surrounding medium through electroluminescence that generates radiation to the far field. The concept of electroluminescent cooling has since been further explored in a number of publications.[21–26] For example, in Ref. 26, a realistic single-quantum well InGaN/GaN LED is investigated by including all relevant heat transfer mechanisms. With a built-in quantum well polarization field, the internal temperature rise can be potentially reduced up to 20% and an electrical efficiency of 1.02 is predicted. However, there has not been an experimental demonstration of actual cooling from electroluminescence, due in part to the presence of non-radiative recombination that limits the radiative efficiency of most semiconductors, as well as the difficulty of extracting photons out of high-index semiconductors.

In Ref. 27, Chen *et al.* proposed to overcome the difficulties of far-field electroluminescent cooling by considering a near-field configuration. The configuration in Ref. 27 consists of two planar semiconductor regions separated by a vacuum gap with a sub-wavelength size. The two planar regions are maintained at different temperatures and undergo electromagnetic energy exchange between them. A positive bias is applied to the cold side in order to generate heat flow from the cold side to the hot side. Reference 27 showed that this near-field configuration can significantly mitigate the detrimental effects of non-radiative recombination. In addition, it was also noted that to achieve significant cooling in the near-field, the sub-bandgap heat transfer due to phonon-polariton needs to be suppressed.[27]

As an example for the near-field electroluminescent cooling, Ref. 27 considered the use of InAs as the cold side with a temperature of 290 K and InSb as a hot side with a temperature of 300 K, and theoretically predicted a cooling power density of approximately $100\ \mathrm{W/m^2}$ and a coefficient of performance (COP) that is 5.7% of the Carnot limit. Subsequently, Liu and Zhang[28] considered a system with GaSb as the cold side, and Ge as the hot side, and predicted a maximum cooling power density of $11.56\ \mathrm{kW/m^2}$ with a 10 nm vacuum gap. Neither of these cooling power densities, however, is competitive against the thermoelectric devices operating at similar temperature ranges.

In this paper, we show that the performance of the previous near-field electroluminescent cooling systems can be

a)eliy@eecs.berkeley.edu
b)shanhui@stanford.edu

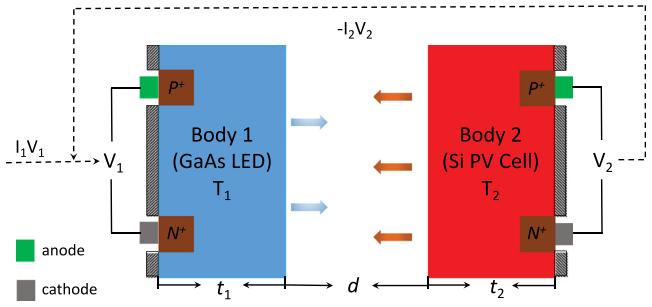

FIG. 1. A near-field electroluminescent cooling device consisting of a LED (made of GaAs) at temperature T_1 and a PV cell (made of Si) at temperature T_1, separated by a vacuum gap with size d, and $T_1 < T_2$. The thicknesses of the two bodies are t_1 and t_2. Both bodies are backed with perfectly reflecting mirrors in order to prohibit emission to the back sides. The voltages applied on the LED is V_1, and a result of a net photo flux from the LED to the PV cell, the PV cell may have a voltage V_2. The generated electric power $-I_2V_2$ can be fed back as part of the injected external electric power I_1V_1 into the LED, where I_1 and I_2 are the current densities in bodies 1 and 2 defined in Eqs. (6) and (7). The arrows indicate the direction of emission from the GaAs LED and the Si PV cell.

significantly improved by using GaAs and Si as the cold and hot sides, respectively, as shown in Fig. 1. GaAs has greatly reduced Auger recombination as compared to both GaSb and InAs. Also, Si, being a non-polar semiconductor, does not possess an optically active phonon-polariton so that the parasitic sub-bandgap phonon-polariton heat leakage can be significantly suppressed.[28,29] Moreover, we show that the system efficiency can be further improved by combining electroluminescent cooling with photovoltaic (PV) power recovery, where the electric power generated in the Si photovoltaic cell is fed back to the GaAs light emitting diode. This is the inverse of the thermophotonic heat engine proposed by Green.[30] Our theoretical calculations show that the system can have a cooling power density in the order of $10^5\ \mathrm{W/m^2}$, which is comparable to what can be achieved in thermoelectric cooling.

The electroluminescent cooling device as we study here seeks to manipulate photon-based heat flow. Since thermal radiation at 300 K has a wavelength of near 10 μm, one might think that an electroluminescent cooling device operating near room temperature may also require the use of narrow-band gap semiconductors. Here, somewhat counter-intuitively, we show that a practical choice for electro-luminescent cooling in fact is to use a wider bandgap semiconductor, where the Auger recombination is far lower as compared to narrow-bandgap semiconductors.

The paper is organized as follows: In Sec. II, we present the theoretical formalism. In Sec. III, we present and discuss the results obtained by exact numerical calculation which takes into account various nonidealities and compare our device to thermoelectric coolers. We summarize and conclude in Sec. IV.

II. THEORETICAL FORMALISM

A. Configuration

Throughout the paper, we consider the configuration as shown in Fig. 1, which consists of two semiconductor bodies. Both bodies consist of a PN junction with small heavily doped P^+ and N^+ regions at the backside that provide electric contact, and an active region which can be either lightly doped or intrinsic. The active regions face each other across the vacuum gap. We also assume that the two bodies only emit to each other through the surfaces on the vacuum gap side as indicated by the colored arrows in Fig. 1, and there is no emission on the edges. Body 1 consists of GaAs, maintained at a temperature T_1, subject to a bias V_1. Body 2 consists of Si, maintained at a temperature T_2, subject to a bias V_2. A positive sign of the voltage corresponds to forward bias of the junction. We assume that $T_1 < T_2$. The objective of our device is to pump heat from the colder GaAs body to the hotter silicon body. For this purpose, in our configuration, both the Si and the GaAs junctions are forward biased, i.e., both V_1 and V_2 are greater than zero. The forward bias on the GaAs junction is (partially) externally provided, and hence the GaAs body operates as a light emitting diode (LED), with the externally provided electric power serving as the power input to the heat pump as required by the Second Law of Thermodynamics. With $V_1 > 0$, there is a net photon flow from the GaAs body to the silicon body, and hence the silicon body operates as a photovoltaic (PV) cell generating a positive V_2 across the silicon junction. The output electric power from the silicon PV cell can be injected back to the GaAs LED, and thus, contributes to the total injected electric power into the GaAs LED. We will show that the use of such photovoltaic power recovery is beneficial for the overall efficiency of electroluminescent cooling device.

Throughout the paper, we choose $T_1 = 280\,\mathrm{K}$ and $T_2 = 330\,\mathrm{K}$. This temperature choice is practical for electroluminescent cooling applications.

B. Detailed balance relations

To model the heat transfer in the system in Fig. 1, we use the standard formalism of fluctuational electrodynamics[31] that has been widely used to treat near-field electromagnetic heat transfer. The detailed theoretical formalism can be found in Ref. 27. Here, we include only those aspects that are essential and are directly relevant for the present paper. In the presence of an external voltage, we treat the current-current correlation functions separately for frequencies above and below band gap, i.e.,[29,32]

$$\langle \boldsymbol{j}_\alpha(\boldsymbol{r},\omega)\boldsymbol{j}^*_\beta(\boldsymbol{r}',\omega')\rangle = \begin{cases} \dfrac{4}{\pi}\omega\Theta(\omega,T,V)\epsilon''_e(\omega)\delta(\boldsymbol{r}-\boldsymbol{r}')\delta(\omega-\omega')\delta_{\alpha\beta} & (\omega \geq \omega_g) \quad (1a) \\ \dfrac{4}{\pi}\omega\Theta(\omega,T,0)\epsilon''_p(\omega)\delta(\boldsymbol{r}-\boldsymbol{r}')\delta(\omega-\omega')\delta_{\alpha\beta} & (\omega < \omega_g), \quad (1b) \end{cases}$$

where α and β label the directions of polarization, $\boldsymbol{r}$ and $\boldsymbol{r}'$ are position vectors, $\delta(\omega-\omega')$ is the Dirac delta function, $\epsilon_e''(\omega)$ and $\epsilon_p''(\omega)$ are the imaginary parts of the dielectric functions that result from interband transitions ($\epsilon_e(\omega)$) and sub-bandgap transitions ($\epsilon_p(\omega)$), respectively, and ω_g is the bandgap frequency

$$\Theta(\omega,T,V)=\frac{\hbar\omega}{\exp\left(\frac{\hbar\omega-qV}{k_BT}\right)-1} \tag{2}$$

is the average photon energy[33] in a single mode at an angular frequency ω, q is the magnitude of the electron's charge, $\hbar$ is the reduced Planck's constant, k_B is the Boltzmann constant, and V is the voltage on the body.

The transferred power density can be directly computed using standard dyadic Green's function technique.[6,7,34] We compute the net energy fluxes from electronic excitations E^e from the LED to the PV cell and the parasitic heat fluxes E^p from the PV cell to the LED due to the phonon-polariton excitations on the GaAs-vacuum interface. These fluxes are obtained by integrating over the appropriate frequency ranges

$$E^e=\int_{\omega_{\rm th}}^{+\infty}[\Theta(\omega,T_1,V_1)-\Theta(\omega,T_2,V_2)]\Phi(\omega)\,d\omega, \tag{3}$$

$$E^p=\int_{0}^{\omega_{\rm th}}[\Theta(\omega,T_2,0)-\Theta(\omega,T_1,0)]\Phi(\omega)\,d\omega, \tag{4}$$

where $\Phi(\omega)$ is the transmission coefficient integrated over the lateral wave vectors $\boldsymbol{k}_{\parallel}$ at the frequency ω,[27] and can be computed through a scattering matrix formalism[35] or by directly integrating the contributions from the current sources defined in Eqs. (1a) and (1b) over the volume of the emitting body.[1] A similar calculation also yields the net above-bandgap photon flux between the two bodies as

$$F=\int_{\omega_{\rm th}}^{+\infty}\frac{\Theta(\omega,T_1,V_1)}{\hbar\omega}\Phi(\omega)\,d\omega-\int_{\omega_{\rm th}}^{+\infty}\frac{\Theta(\omega,T_2,V_2)}{\hbar\omega}\Phi(\omega)\,d\omega. \tag{5}$$

We denote the first and the second terms in Eq. (5) as $F_{1\to2}$ and $F_{2\to1}$, respectively. For an ideal semiconductor, there is no absorption of light for frequencies immediately below the bandgap frequency ω_g, and therefore, one would choose $\omega_{\rm th}=\omega_g$ in Eqs. (3)–(5). In the present case, however, we note that for both GaAs and Si, in the frequency range immediately below the bandgap frequency ω_g, the imaginary part of the dielectric function is not exactly zero due to the existence of Urbach tail.[36] Therefore, in the numerical evaluations of Eqs. (3)–(5), we choose $\omega_{\rm th}=2.08\times10^{15}$ rad/s that is slightly below ω_g. We note that for the above formalism to be valid, the maximum value for V_1 needs to be lower than $\hbar\omega_{\rm th}/q$. Thus, in this paper, we set the maximum value of V_1 to be 1.35 V. In addition, both the contributions of propagating and evanescent waves are included in this calculation. However, in the near-field regime, the contributions from evanescent waves dominate.

For LED, the photons above band gap come from radiative recombination. Therefore, the above-bandgap photon flux as calculated in Eq. (5) is the net radiative recombination rate. The enhancement of radiative heat flux in the near field thus translates to an enhancement of radiative recombination rate in this system.

Having obtained the net energy fluxes and the net photon fluxes, one can evaluate the performance of the device by calculating the cooling power density and the efficiency. For the currents, we use the sign convention that a positive current corresponds to the flow of positive charge from P^+ anode through the semiconductor to the N^+ cathode. Also, when referring to unit area, including either explicitly or implicitly in the definition of current density or power density, we refer to the unit area of the semiconductor surface facing the vacuum gap. Then, the current densities in the LED and the PV cell are given by

$$I_1=q(F+R_1), \tag{6}$$

$$I_2=q(-F+R_2), \tag{7}$$

where R_a is the total nonradiative recombination rate per unit area for body a ($a=1,2$) and F depends on the voltages on both bodies as indicated by Eq. (5). Assuming that the system has no parasitic photon absorption, i.e., all absorption of photons occur in the Si and GaAs active regions, we define the luminescent efficiency (η_l) for the LED as the ratio of radiative recombination rate to the total recombination rate, i.e.,

$$\eta_l=\frac{F_{1\to2}}{F_{1\to2}+R_1}\times100\%, \tag{8}$$

where the numerator describes the radiative recombination rate in GaAs and the denominator describes the total recombination rate.

We define the net cooling power density for the system as

$$Q_c=(E^e-E^p)-I_1V_1, \tag{9}$$

where the first term describes the net heat flow across the vacuum gap, and the second term refers to the total injected power into the LED. Having obtained the cooling power density, we compute the cooling coefficient of performance (COP), defined as the ratio of the net cooling power density obtained in Eq. (9) to the total power density required from the outside into the LED

$$\mathrm{COP}=\frac{Q_c}{I_1V_1+I_2V_2}, \tag{10}$$

where the denominator represents the extra power density needed from the outside of the device in the presence of the recollected electric power density I_2V_2. In contrast to Ref. 27, which focused on the $V_2=0$ case, here, we assume that the PV cell can have a non-zero forward bias generated by the incoming flux from the LED. In our calculation in this paper, we maximize the COP using Eq. (10) over all possible V_2 values. For comparison purposes, we further normalize the COP thus obtained numerically with respect to by the

Carnot limit of $T_1/(T_2 - T_1)$, which is 5.6 for our choice of temperatures.

C. Nonradiative recombination

A key consideration in electroluminescent cooling is to reduce the non-radiative recombination. Here, we provide a brief discussion of non-radiative recombination processes in GaAs and Si. For both GaAs and Si, we consider Auger recombination and bulk Shockley-Read-Hall (SRH) recombination. Hence, we set R_a ($a = 1, 2$ denoting the two bodies) in Eqs. (6) and (7) to[37,38]

$$R_a = (C_{n,a} n_a + C_{p,a} p_a)(n_a p_a - n_{i,a}^2) t_a + A_a \frac{n_a p_a - n_{i,a}^2}{n_a + p_a + 2n_{i,a}} t_a. \tag{11}$$

In Eq. (11), the first and second terms refer to the Auger and SRH processes, respectively. $C_{n,a}$ and $C_{p,a}$ are the Auger recombination coefficients for two-electron and two-hole processes of body a ($a = 1, 2$), respectively. n_a and p_a are electrons and holes density of body a, respectively. $n_{i,a}$ is the intrinsic carrier concentration for body a. t_a is the thickness of body a, and A_a is the SRH recombination coefficient of body a and is related to the SRH lifetime $\tau_{\mathrm{SRH},a}$ through $A_a = 1/\tau_{\mathrm{SRH},a}$.

The non-radiative recombination rate and the luminescent efficiency in GaAs strongly depends on both the doping concentration and on the applied voltage. To determine the optimal doping concentration, we follow Ref. 39 and assume a p-doped GaAs in the low injection regime, i.e., $n_1 \ll p_1 \approx N_A$ and a simple radiative recombination rate expressed as Bn_1N_A where B is the radiative recombination coefficient, Eq. (8) reduces to a bias-independent form

$$\eta_l|_{n_1 \ll p_1} = \frac{BN_A}{A_1 + BN_A + C_{p,1}N_A^2}. \tag{12}$$

This results in $N_A = \sqrt{A_1/C_{p,1}}$ where Eq. (12) reaches its maximum.

In the case of low injection where V_1 is small, the hole concentration $p_1 \approx N_A$. Therefore, n_1 is small and scales with $e^{\frac{qV_1}{k_B T_1}}$. As a result, the SRH process dominates. When V_1 is large where low injection approximation fails, both n_1 and p_1 scales with $e^{\frac{qV_1}{2k_B T_1}}$. Thus, the Auger recombination rate scales as $e^{\frac{3qV_1}{2k_B T_1}}$ and becomes significant. As a result of the competing non-radiative processes inside GaAs, to achieve net cooling, the choice of voltage V_1 is therefore essential. For the cooling device as we consider here, and for the range of voltages we use in the paper, the voltage that optimizes the COP does not necessarily correspond to the low injection condition as discussed above, but as we will see, this choice of N_A results in a very good luminescent efficiency.

For Si, as we will see below that the injected photon density is actually very high. In the comparison to solar cells, this corresponds to a few thousand suns. Therefore, it is best to take Si as intrinsic to minimize the Auger recombination.

In the calculation in Sec. III, the intrinsic carrier densities for GaAs and Si are $n_{i,1} = 2.8 \times 10^5\,\mathrm{cm}^{-3}$ (Refs. 38 and 40) and $n_{i,2} = 1.4 \times 10^{10}\,\mathrm{cm}^{-3}$ (Refs. 40 and 41) for the temperatures that we consider here. The Auger recombination coefficient of GaAs is $C_1 = 7 \times 10^{-30}\,\mathrm{cm}^6\,\mathrm{s}^{-1}$, with $C_{n,1}$ and $C_{p,1}$ each equal to $C_1/2$.[42] The Auger recombination coefficient of Si is $C_{n,2} + C_{p,2} = 1.4 \times 10^{-30}\,\mathrm{cm}^6\,\mathrm{s}^{-1}$.[40,43] At small t_1, the radiative recombination rate increases as t_1 increases, and for large t_1, the radiative recombination rate saturates. On the other hand, the non-radiative recombination rate defined in Eq. (11) scales proportionally to t_1. Therefore, there is an optimal t_1 that maximizes the cooling power density in the presence of non-radiative recombination. We find the optimal $t_1 = 500\,\mathrm{nm}$ for the GaAs LED. With this thickness value, the SRH lifetime for GaAs is estimated to be $\tau_{\mathrm{SRH},1} = 16.7\,\mu\mathrm{s}$ assuming GaInP passivation.[44] Using these parameters, we optimize the doping level for GaAs to be $1.31 \times 10^{17}\,\mathrm{cm}^{-3}$ for maximum luminescent efficiency consideration through $N_A = \sqrt{A_1/C_{p,1}}$. In addition, in order to maximize the absorption by Si, we choose a thick Si body with thickness $t_2 = 50\,\mu\mathrm{m}$, and the bulk SRH lifetime $\tau_{\mathrm{SRH},2}$ is 35 ms.[45]

III. NUMERICAL RESULTS

In the following calculation of near-field heat transfer, the frequency-dependent dielectric functions for GaAs and Si are obtained from Refs. 42, 46, and 47 and linearly interpolated. We plot the dielectric functions for GaAs and Si for the above-bandgap and sub-bandgap regions as a function of wavelength in Figs. 2(a)–2(d). We notice that in the sub-bandgap frequency range, the imaginary part of dielectric function of GaAs [Fig. 2(b)] has a peak at a wavelength of 37.5 μm, corresponding to the phonon-polariton of GaAs. By comparison, for Si [Fig. 2(d)], there is no such phonon-polariton peak since silicon is a non-polar material, and hence, the imaginary part of the dielectric function in the sub-bandgap region remains relatively small in the order of 10^{-4}. The absence of the phonon-polariton peak in the sub-band gap region is an important advantage in the present

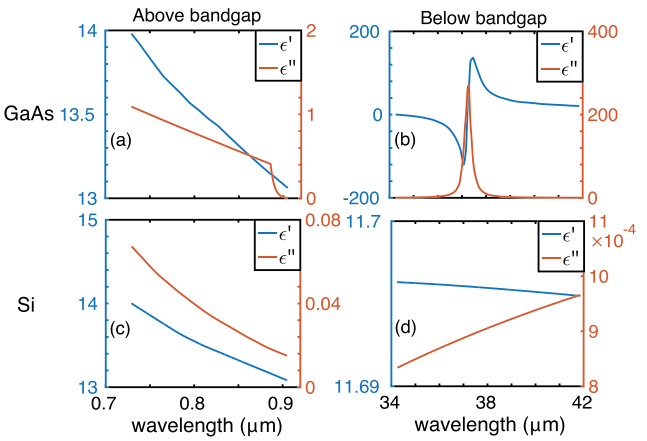

FIG. 2. (a) and (c) Dielectric functions for GaAs and Si for wavelengths in the above-bandgap region of GaAs. (b) and (d) Dielectric function for GaAs and Si for wavelengths in the sub-bandgap region of GaAs. The blue and red curves correspond to the real and imaginary parts of the dielectric functions, respectively.

configuration as compared to Ref. 27, where it was shown that the existence of sub-bandgap phonon-polariton leads to a strong sub-bandgap heat transfer in the near-field region that degrades the cooling performance.

In this section, we apply the formalism introduced in Sec. II B to our configuration, taking into account the non-radiative recombination processes described in Sec. II C. In Sec. III A, we first discuss the performance of our device in the absence of photovoltaic power recovery ($V_2 = 0$), which resembles the setup in Ref. 27. In Sec. III B, we consider the impact of photovoltaic power recovery, where the part of power generated by the Si PV cell is fed back to the GaAs LED. In Sec. III C, we compare our device to thermoelectric coolers. In Sec. III D, we discuss the detrimental effects of the existence of a thin SiO_2 layer on the silicon surface on the performance of our device.

A. Performance in the absence of photovoltaic power recovery

We first compute the cooling power density and the COP in the absence of photovoltaic power recovery. This is done by shorting the PV cell, i.e., by setting $V_2 = 0$. In Fig. 3(a), we show the cooling power density as a function of the LED bias V_1 for $d = 10\,\text{nm}$ and $10\,\mu\text{m}$ in blue and red curves, respectively. At $V_1 = 0$, the net heat flow should go from the hot side to the cold side, as required by the Second Law of Thermodynamics, and hence, the net cooling power density is negative. When V_1 is small, the cooling power density remains negative because of the existence of sub-bandgap heat transfer. The cooling power becomes positive at $V_1 \approx 1.02\,\text{V}$. As V_1 further increases, the cooling power density increases drastically as a function of V_1, reaching a peak of $6.96 \times 10^5\,\text{W/m}^2$ at $V_1 = 1.35\,\text{V}$. For this gap separation, we do not observe a decrease of cooling power density because for the voltage range that we have considered here, the radiative recombination process always dominates over the competing non-radiative recombination processes.

In terms of cooling power density, with a 10 nm vacuum gap, the results here are about three orders of magnitude higher as compared to Ref. 27, which used InAs and InSb as the semiconductors, and about one order of magnitude higher as compared to Ref. 28, which used GaSb and Ge as the semiconductors. The improved performance here arises from the use of GaAs, which has a wider bandgap and, therefore, a far lower Auger recombination rate.

The use of near-field heat transfer is essential for the cooling performance that we observe here. As a direct comparison, in Fig. 3(a) we plot as the red curve the cooling power density in a far-field setup where the LED and the PV cell are separated by a vacuum gap of $10\,\mu\text{m}$ that is much larger than the bandgap wavelength. Significantly reduced refrigeration power density is observed as a result of the reduced radiative recombination rate in GaAs when the GaAs LED and the Si PV are separated in the far-field region. In general, it is difficult to observe large cooling power in the far-field region in the simple planar geometry. One may significantly improve the cooling performance in the far-field region with the use of rear surface texturing that

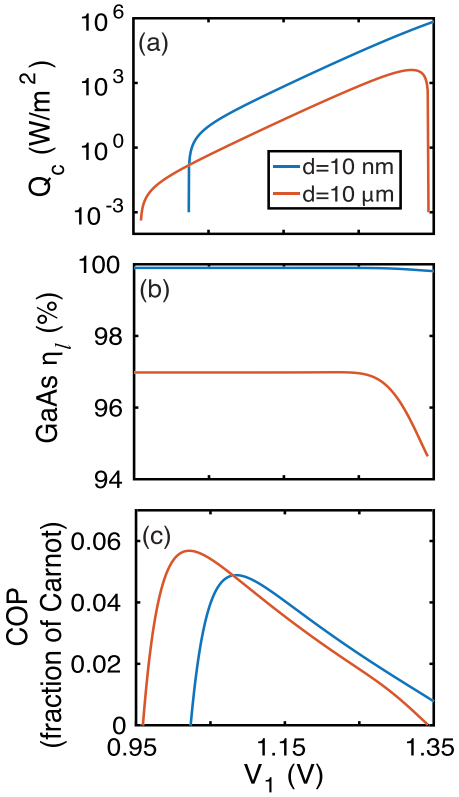

FIG. 3. (a) Cooling power density as a function of LED voltage V_1 for the configuration shown in Fig. 1 with the PV cell short-circuited. Red and blue curves correspond to vacuum gap sizes of $d = 10\,\text{nm}$ and $10\,\mu\text{m}$, respectively. (b) Luminescent efficiency (η_l) as a function of V_1 for $d = 10\,\text{nm}$ and $10\,\mu\text{m}$ in blue and red curves, respectively. (c) COP normalized with respect to the Carnot efficiency as a function of V_1 for $d = 10\,\text{nm}$ and $10\,\mu\text{m}$ in blue and red curves, respectively.

facilitates the extraction of photons, which greatly enhances radiative recombination over non-radiative recombination.

To better analyze the significant difference in cooling performance between the near-field and far-field regimes, we plot the luminescent efficiency of GaAs as a function of V_1 for $d = 10\,\text{nm}$ and $10\,\mu\text{m}$ in Fig. 3(b). Since the SRH recombination is small compared to radiative recombination, the luminescent efficiency is flat for a large range of V_1. However, in the far-field case ($d = 10\,\mu\text{m}$), as V_1 approaches to the bandgap, the luminescent efficiency starts to drop because of the significant Auger recombination. In contrast, in the near-field case ($d = 10\,\text{nm}$), the luminescent efficiency remains almost unchanged at a high value as V_1 increases up to 1.35 V. In the near-field regime, the radiative recombination rate is significantly enhanced, leading to the enhanced luminescent efficiency. Such an enhancement of luminescent efficiency is essential for the observation of significant cooling in the presence of realistic non-radiative recombinations.

We plot the COP as a function of LED bias V_1 for $d = 10\,\text{nm}$ and $10\,\mu\text{m}$ in Fig. 3(c). Due to the significant enhancement of sub-bandgap parasitic heat transfer in the near-field regime, we observe that the COP in the far field has a higher peak value than that in the near field. However, the near-field case has a higher COP for larger biases, because of the enhanced radiative recombination rate in the LED. In general, being able to operate at higher voltage, as we observe for

the near-field case as compared to the far-field case, is advantageous since at a higher voltage we expect a higher cooling power density.

B. Performance with photovoltaic power recovery

In general, when there is a net photon flux from the LED to the PV cell, a non-zero positive voltage V_2 on the PV cell can be generated, and the electric power generated from the PV cell can be fed back into the LED, thus reducing the required external power that is injected into the LED. On the other hand, a non-zero positive voltage on the PV cell results in a higher heat back flow from the PV cell to the LED. As a balance of these competing effects, there is an optimal V_2 in order to achieve the maximal COP.

In Fig. 4(a), we plot the optimal COP as a function of the LED voltage V_1 for vacuum gaps $d = 10\,\text{nm}$ and $10\,\mu\text{m}$ as red and blue curves, respectively. For each value of V_1 and gap size in Fig. 4(a), we optimize V_2 to reach the optimal COP. The values of V_2 thus obtained as a function of V_1 for the two gap sizes, are shown in Fig. 4(b). Compared to Fig. 3(c), we observe a significant increase of COP for both the far-field and near-field cases. Also, in Fig. 4(b), we observe that the optimal V_2 is far smaller as compared to the bandgap of Si. Therefore, at the optimal V_2, the net cooling power is unaffected since the back flow of heat from the PV cell back to the LED is still significantly smaller as compared to power carried by the photon flow from the LED to the PV cell. Thus, the photovoltaic power recovery can be used to significantly enhance the COP without degrading the cooling power.

The results here represent significant improvements in terms of power density as compared to previous works. Chen *et al.*[27] discussed a structure with the InAs as the LED and the InSb as the PV, with a peak cooling power density of $91\,\text{W/m}^2$. Liu and Zhang[28] discussed a structure with GaSb as the LED and Ge as the PV cell, with a peak cooling power density of $1.16 \times 10^4\,\text{W/m}^2$. The significant power density improvement in our present work occurs from the significantly reduced Auger recombination rate in GaAs, which results in a much higher radiative recombination yield. At the peak power density, which corresponds to $V_1 = 1.35\,\text{V}$, the luminescent efficiency for the GaAs system is 99.8%, whereas for the InAs and the GaSb systems, the luminescent efficiencies at the maximum power point are approximately 62.8% and 99.1%, respectively.

We notice that even in the presence of photovoltaic power recovery, the maximum COP shown in Fig. 4 is still much lower than the Carnot limit under these temperatures. In the absence of non-radiative recombination, the Carnot limit is reached when the applied voltage is close to the threshold.[27] At such a low applied voltage, the cooling power density is very small, and the system is, therefore, particularly susceptible to the detrimental effect of parasitic heat transfer below the band gap. In order to achieve a high COP close to Carnot limit, further engineering is required to reduce the parasitic heat transfer in the sub-bandgap regime.

C. Comparison with thermoelectric cooler

Cooling devices, in general, exhibit a trade-off between the COP and the cooling power density. Therefore, a reasonable way to compare the performances of different cooling devices is to compare their cooling power density at the same COP. For this purpose, in Fig. 5, we plot the COP as a function of the cooling power density as the LED bias V_1 varies, for the two cases with the vacuum gap sizes of $d = 10\,\text{nm}$ and $d = 10\,\mu\text{m}$, corresponding to the near-field and far-field cases, respectively. For each LED bias V_1, we plot the COP and the power density at the optimal PV cell bias V_2 as

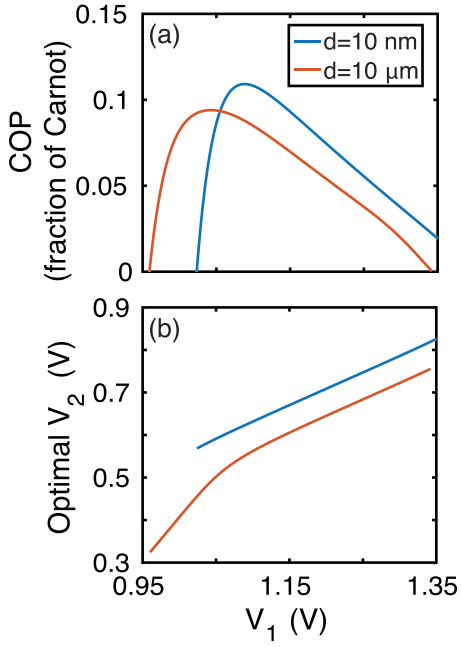

FIG. 4. (a) COP normalized with respect to the Carnot efficiency as a function of V_1 with photovoltaic power recovery from the PV cell for vacuum gaps $d = 10\,\text{nm}$ and $10\,\mu\text{m}$ in blue and red curves, respectively, for $T_1 = 280\,\text{K}$ and $T_2 = 330\,\text{K}$. (b) The optimal bias V_2 for the PV cell for each LED bias V_1 value where there is net cooling. The red and blue curves correspond to vacuum gaps $d = 10\,\text{nm}$ and $10\,\mu\text{m}$, respectively.

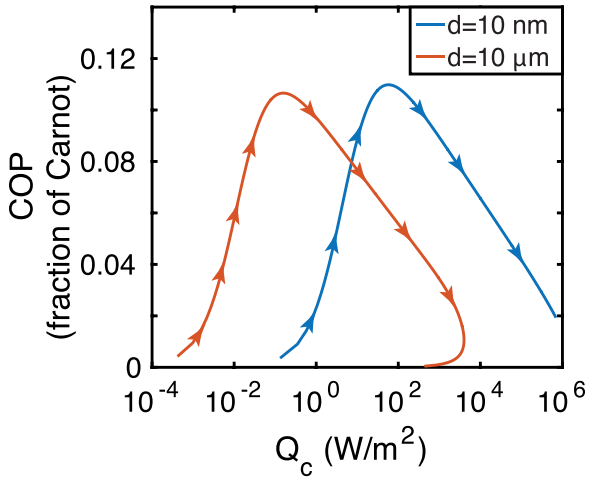

FIG. 5. COP normalized with respect to the Carnot limit as a function of cooling power density, for the device configuration shown in Fig. 1. Each data point in the plot corresponds to a particular LED bias V_1 with a corresponding optimal PV bias V_2. The arrow indicates the direction of increasing V_1. The blue and red curves correspond to near-field vacuum gap $d = 10\,\text{nm}$ and $10\,\mu\text{m}$, respectively.

discussed earlier. At the same COP, the near-field configuration has a much higher cooling power density as compared to the far-field configuration. For both cases, the optimal cooling power density and the optimal COP occur at different LED bias V_1. For the near-field case with a gap size of $d = 10\,\text{nm}$, the structure reaches an optimal COP = 11.0% of the Carnot limit with a cooling power density of $57.3\,\text{W/m}^2$ at $V_1 = 1.09\,\text{V}$. It reaches an optimal cooling power density of $6.96 \times 10^5\,\text{W/m}^2$ with a COP of 1.9% of the Carnot limit at $V_1 = 1.35\,\text{V}$. Whereas for the far-field case with a gap size of $d = 10\,\mu\text{m}$, the optimal COP is 10.7% of Carnot with $Q_c = 0.161\,\text{W/m}^2$ at $V_1 = 1.03\,\text{V}$, and optimal cooling power density is $4.00 \times 10^3\,\text{W/m}^2$ at a COP with the value of 1.1% of the Carnot limit at $V_1 = 1.32\,\text{V}$. Therefore, the main benefit of the operating in the near-field regime is that it allows one to reach a power density that is about two orders of magnitude higher at a comparable COP as compared to the far-field case.

The concept of electroluminescent cooling provides an interesting alternative approach for solid-state cooling. Therefore, it would be useful to compare the performance predicted here to the performance of thermoelectric cooler. Reference 48 presents a summary for the commercially available thermoelectric modules. Most of the devices provide a maximum cooling power density at the order of $10^4\,\text{W/m}^2$ when the hot side is maintained at room temperature. Our device can provide an order of magnitude improvement in cooling power as compared with such thermoelectric devices. In terms of COP, a thermoelectric cooler with $ZT = 1.0$, operating at the same temperature difference $\Delta T = 50\,\text{K}$ as our device, exhibits a COP of 10% of the Carnot limit. This is comparable to the COP of our device. The results presented here point to the important potential of electroluminescent cooling devices. In this paper, we use a planar geometry for near-field heat transfer. The performance of our device may be further improved with more sophisticated geometry optimized for enhancing near-field heat transfer.[49,50]

D. Impact of the SiO_2 layer on the Si surface

In practice, silicon and GaAs usually have a thin layer of coating for passivation purposes.[39,51] For example, GaAs can be passivated with GaInP[39] and silicon always has a silicon dioxide (SiO_2) coating.[51] The existence of the coating can result in a parasitic heat flow, since all the materials in the coating are polar materials that support photon-polariton excitations. On the other hand, since GaAs already has a strong phonon-polariton response that is already taken into account in the previous simulation, the presence of GaInP passivation layer should not significantly affect the heat transfer. Therefore, here we ignore the effects of GaInP phonon-polaritons and mainly focus on the heat flow from the Si side directly to the GaAs side due to the surface phonon-polariton of SiO_2. For amorphous SiO_2, its two surface phonon-polaritons are located at the wavelengths of $9.3\,\mu\text{m}$ and $21.7\,\mu\text{m}$, which misalign with the surface phonon-polariton of GaAs. Therefore, the backward heat flow due to an oxide layer is not very significant. To investigate the effect of the oxide layer, we perform numerical calculations by fixing the vacuum gap $d = 10\,\text{nm}$ and varying the thickness of SiO_2 layer on silicon. We show the cooling power density as a function of SiO_2 thickness in Fig. 6(a). When the thickness of SiO_2 increases, the cooling power density decreases. However, even with a 20 nm SiO_2 layer on top of Si, the cooling power density can still be as high as $5.24 \times 10^5\,\text{W/m}^2$ at LED bias $V_1 = 1.35\,\text{V}$. In Fig. 6(b), we plot the maximum COP as a function of the thickness of the SiO_2 layer. The COP also decreases as the thickness increases. However, we still observe a COP = 4.3% of the Carnot limit when the SiO_2 thickness is 20 nm. Therefore, the significant performance of our device still persists even in the presence of a thin SiO_2 layer.

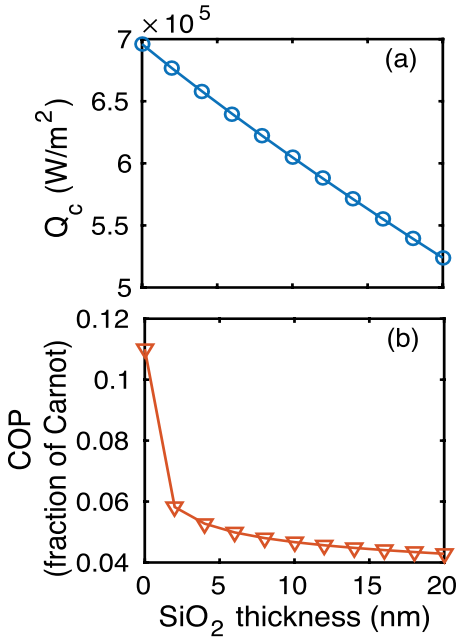

FIG. 6. The performance of the configuration of the device in Fig. 1, except that a SiO_2 layer is added on the silicon surface facing the vacuum gap. The size of the vacuum gap between the LED and the PV cell is fixed at 10 nm. (a) Maximum cooling power density and (b) maximum COP as a function of the thickness of the SiO_2 layer on the silicon PV cell. Good performance requires a SiO_2 layer thickness of less than 2 nm.

IV. CONCLUSION

In conclusion, we introduce a new device configuration that significantly improves the performance of the near-field electroluminescent cooling device as introduced in Ref. 27 and further studied in Ref. 28. This device configuration uses GaAs, which has significantly reduced Auger recombination as compared with narrow-bandgap semiconductors used in Ref. 27, and uses Si that does not have surface phonon-polariton, which results in significant suppression of parasitic backward heat flow. We also combine the concept of near-field electroluminescent cooling with the idea of photovoltaic power recovery.[30] As a result, we numerically demonstrate orders of magnitude improvement in the performance of near-field electroluminescent cooling device. The peak cooling power density of this system is $6.96 \times 10^5\,\text{W/m}^2$,

which exceeds standard thermoelectric coolers operating in the same temperature range while maintaining a similar COP. Our work points to the significant potential, where the combination of near-field heat transfer and active semiconductor devices can lead to new possibilities for heat manipulation.

ACKNOWLEDGMENTS

This work was supported by the DOE "Light-Material Interactions in Energy Conversion" Energy Frontier Research Center under Grant No. DE-SC0001293.

[1]D. Polder and M. Van Hove, Phys. Rev. B **4**, 3303 (1971).
[2]J. B. Pendry, J. Phys.: Condens. Matter **11**, 6621 (1999).
[3]J. J. Loomis and H. J. Maris, Phys. Rev. B **50**, 18517 (1994).
[4]E. Rousseau, A. Siria, G. Jourdan, S. Volz, F. Comin, J. Chevrier, and J. J. Greffet, Nat. Photonics **3**, 514 (2009).
[5]B. Guha, C. R. Otey, C. B. Poitras, S. Fan, and M. Lipson, Nano Lett. **12**, 4546 (2012).
[6]M. Krüger, T. Emig, and M. Kardar, Phys. Rev. Lett. **106**, 210404 (2011).
[7]C. R. Otey and S. Fan, Phys. Rev. B **84**, 245431 (2011).
[8]R. Messina and M. Antezza, Europhys. Lett. **95**, 61002 (2011).
[9]A. Narayanaswamy and G. Chen, Phys. Rev. B **77**, 075125 (2008).
[10]A. W. Rodriguez, M. T. H. Reid, J. Varela, J. D. Joannopoulos, F. Capasso, and S. G. Johnson, Phys. Rev. Lett. **110**, 014301 (2013).
[11]C. R. Otey, L. Zhu, S. Sandhu, and S. Fan, J. Quantum Spectrosc. Radiat. Trans. **132**, 3 (2014).
[12]A. I. Volokitin and B. N. J. Persson, Rev. Mod. Phys. **79**, 1291 (2007).
[13]A. Narayanaswamy and G. Chen, Appl. Phys. Lett. **82**, 3544 (2003).
[14]B. Zhao, L. Wang, Y. Shuai, and Z. M. Zhang, Int. J. Heat Mass Transfer **67**, 637 (2013).
[15]O. Ilic, M. Jablan, J. D. Joannopoulos, I. Celanovic, and M. Soljačić, Opt. Express **20**, A366 (2012).
[16]M. Laroche, R. Carminati, and J.-J. Greffet, J. Appl. Phys. **100**, 063704 (2006).
[17]M. Francoeur, M. P. Meng, and R. Vaillon, Appl. Phys. Lett. **93**, 043109 (2008).
[18]S. Basu, Z. M. Zhang, and C. J. Fu, Int. J. Energy Res. **33**, 1203 (2009).
[19]K. Park, S. Basu, W. King, and Z. Zhang, J. Quantum Spectrosc. Radiat. Transfer **109**, 305 (2008).
[20]J. Tauc, Czech. J. Phys. **7**, 275 (1957).
[21]P. Berdahl, J. Appl. Phys. **58**, 1369 (1985).
[22]S.-Q. Yu, J.-B. Wang, D. Ding, S. R. Johnson, D. Vasileska, and Y.-H. Zhang, Proc. SPIE **6486**, 648604 (2007).
[23]O. Heikkil, J. Oksanen, and J. Tulkki, J. Appl. Phys. **107**, 033105 (2010).
[24]P. Santhanam, D. J. Gray, and R. J. Ram, Phys. Rev. Lett. **108**, 097403 (2012).
[25]P. Santhanam, D. Huang, R. J. Ram, M. A. Remennyi, and B. A. Matveev, Appl. Phys. Lett. **103**, 183513 (2013).
[26]J. Piprek and Z.-M. Li, Opt. Quantum Electron. **48**, 472 (2016).
[27]K. Chen, P. Santhanam, S. Sandhu, L. Zhu, and S. Fan, Phys. Rev. B **91**, 134301 (2015).
[28]X. Liu and Z. M. Zhang, Nano Energy **26**, 353 (2016).
[29]K. Chen, P. Santhanam, and S. Fan, Appl. Phys. Lett. **107**, 091106 (2015).
[30]N.-P. Harder and M. A. Green, Semicond. Sci. Technol. **18**, S270 (2003).
[31]S. M. Rytov, *Theory of Electric Fluctuations and Thermal Radiation* (Air Force Cambridge Research Center, Bedford, MA, 1959).
[32]C. H. Henry and R. F. Kazarinov, Rev. Mod. Phys. **68**, 801 (1996).
[33]P. Würfel, J. Phys. C: Solid State Phys. **15**, 3967 (1982).
[34]W. C. Chew, *Waves and Fields in Inhomogeneous Media* (IEEE, New York, 1995).
[35]D. M. Whittaker and I. S. Culshaw, Phys. Rev. B **60**, 2610 (1999).
[36]S. John, C. Soukoulis, M. H. Cohen, and E. N. Economou, Phys. Rev. Lett. **57**, 1777 (1986).
[37]T. Tiedje, E. Yablonovitch, G. D. Cody, and B. G. Brooks, IEEE Trans. Electron Devices **31**, 711 (1984).
[38]S. Sandhu, Z. Yu, and S. Fan, Opt. Express **21**, 1209 (2013).
[39]D. A. Bender, J. G. Cederberg, C. Wang, and M. Sheik-Bahae, Appl. Phys. Lett. **102**, 252102 (2013).
[40]I. P.-T. Institute, NSM Archive - Physical Properties of Semiconductors, 1998.
[41]M. A. Green, J. Appl. Phys. **67**, 2944 (1990).
[42]O. D. Miller, E. Yablonovitch, and S. R. Kurtz, IEEE J. Photovoltaics **2**, 303 (2012).
[43]U. Strauss, W. W. Rhle, and K. Khler, Appl. Phys. Lett. **62**, 55 (1993).
[44]B. Imangholi, M. P. Hasselbeck, M. Sheik-Bahae, R. I. Epstein, and S. Kurtz, Appl. Phys. Lett. **86**, 081104 (2005).
[45]E. Yablonovitch, D. L. Allara, C. C. Chang, T. Gmitter, and T. B. Bright, Phys. Rev. Lett. **57**, 249 (1986).
[46]M. A. Green and M. J. Keevers, Prog. Photovoltaics **3**, 189 (1995).
[47]E. Palik, *Handbook of Optical Constants of Solids* (Academic Press, New York, 1985).
[48]D. Zhao and G. Tan, Appl. Therm. Eng. **66**, 15 (2014).
[49]V. Fernández-Hurtado, F. J. García-Vidal, S. Fan, and J. C. Cuevas, Phys. Rev. Lett. **118**, 203901 (2017).
[50]H. Chalabi, E. Hasman, and M. L. Brongersma, Phys. Rev. B **91**, 174304 (2015).
[51]M. Morita, T. Ohmi, E. Hasegawa, M. Kawakami, and M. Ohwada, J. Appl. Phys. **68**, 1272 (1990).